P2.6 THE INFLUENCE OF PULSE-FIRING DELAYS ON SONIC ANEMOMETER RESPONSE CHARATERISTICS

Morten Nielsen* and Søren E. Larsen
Risø National Laboratory, Roskilde, Denmark

1. INTRODUCTION

State-of-the-art sonic anemometers deduce the instantaneous wind vector and sound virtual temperature by transit times of sound pulses, travelling back and forth in three measurement paths. To eliminate cross-talk effects, the pulse firings are sequential and, therefore, the instrument response is distorted when the frequency of turbulent perturbations approach that of the measurement cycle. Furthermore, the temperature response is distorted by the sound-path bending caused by the wind component perpendicular to the individual measurement path. Since pulse-timing distortions increase with frequency it is necessary to consider compensating effects of volumetric averaging along the measurement paths, together with the block-averaging and aliasing effects of the discrete sample strategy. The co-spectral response of all signals is modelled for the omni-directional Solent R3 anemometer taking its special instrument geometry and pulse-firing rhythm into account. The pulse-firing sequence implies that the response depends on the instrument orientation relative to the wind direction. The temperature and heat-flux responses are improved relative to those of the preceding R2

2. THE SOLENT R3 ANEMOMETER

The omni-directional Solent R3 anemometer has three intersecting measurement paths arranged with 120° azimuth separation and an inclination angle α= 45°. Each measurement cycle involves six sound pulse firings and it is convenient to express their timing relative to the average firing time, i.e. as $-5\tau, -3\tau, -\tau, \tau, 3\tau, 5\tau$ with τ=0.72 ms. Upward firings occur at times $(4j-1)\tau$ and downward firings occur at times $(4j+1)\tau$, with the measurement path index $j=-1,0,+1$. Unit vectors in the directions of the individual paths are defined by

$$\mathbf{t}_j = \left[\cos(2/3\, j\pi)\cos\alpha, -\sin(2/3\, j\pi)\cos\alpha, \sin\alpha\right] \qquad (1)$$

The projection of the ambient wind vector $\mathbf{u}_s$ on individual measurement paths is $\mathbf{u_{p,j}} = \mathbf{t_j}(\mathbf{u_s} \cdot \mathbf{t_j})$ expressed in an orthogonal coordinate system aligned after the instrument, and wind components normal to measurement paths are $\mathbf{u_{n,j}} = \mathbf{u_s} - \mathbf{u_{p,j}}$. The velocities detected by individual measurement paths are $(u_{-1}, u_0, u_{+1}) = \mathbf{T}\mathbf{u_s}$ and the wind vector is reconstructed by $\mathbf{u}_s = \mathbf{S}\cdot(u_{-1}, u_0, u_{+1})$, where the response matrix **T** is composed by measurement-path unit vectors and the back-projection matrix **S** is the inverse of this. For later use, we define $\mathbf{s_j}$ as the column vectors of **S**. In order to relate response characteristics to boundary-layer theory, we express the wind vector in the instrument coordinate system $\mathbf{u}_s = \mathbf{R}\,\mathbf{u}$ by the wind-aligned vector $\mathbf{u} = (\overline{u}+u', v', w')$ and the rotation matrix **R**. Taking the average of measurements by individual transducer pairs minimizes temperature distortion by probe deformation.

3. RESPONSE MODEL

3.1 *Effects of pulse delays*

Larsen *et al.* (1993) approximated the velocity and temperature responses of a single sonic anemometer path by

$$\begin{aligned} u'_{\mathrm{p,s}} &= \frac{1}{2a}\left(T'_{\uparrow} - T'_{\downarrow}\right) + \frac{1}{2}\left(u'_{\mathrm{p},\uparrow} + u'_{\mathrm{p},\downarrow}\right) - \frac{1}{2}\frac{\overline{u}_{\mathrm{n}}}{c}\left(u'_{\mathrm{n},\uparrow} - u'_{\mathrm{n},\downarrow}\right) \\ T' &= \frac{1}{2}\left(T'_{\uparrow} + T'_{\downarrow}\right) + \frac{a}{2}\left(u'_{\mathrm{p},\uparrow} - u'_{\mathrm{p},\downarrow}\right) - \frac{a}{2}\frac{\overline{u}_{\mathrm{n}}}{c}\left(u'_{\mathrm{n},\uparrow} + u'_{\mathrm{n},\downarrow}\right) \end{aligned} \qquad (2)$$

where T is temperature, c is sound velocity, and u_p and u_n denotes wind components in parallel and normal to the measurement path. Mean values and perturbations are marked with overbars and primes, arrows ↑ and ↓ and refer to the upward and downward pulse firings, index s refers to sonic response, and the parameter is defined by $a \equiv 2T/c \approx 1.8\ \mathrm{K\,sm^{-1}}$. Temperature distortion by sound path bending by cross wind (Kaimal and Gaynor 1991) is included in this formula. The response characteristics were modelled by Fourier expansion of all variables x in (2) taking time delays into account by

$$x_1 = \int dZ_x(\omega) e^{i\omega(t-\tau)} \quad x_2 = \int dZ_x(\omega) e^{i\omega(t+\tau)} \qquad (3)$$

where the time lag between pulses is 2τ. The response expressions were translated from exponential to trigonometric functions and response spectra were calculated by insertion of theoretical power and cross spectra. Applying this method for the Solent R3 system we must rotate the wind vector to the instrument

* *Corresponding author address*: Morten Nielsen, Risø National Laboratory, Wind Energy Department, P.O. Box 49, 4000 Roskilde, Denmark. E-mail: n.m.nielsen@risoe.dk

coordinate system and split it into components parallel and normal to individual measurement paths. The temperature signal becomes:

$$dZ_{T,S}(\omega) = \tag{4}$$
$$\frac{1}{3}\Bigg\{\frac{1}{2}\sum_{j=-1}^{+1}\left[e^{i(4j-1)\omega\tau}+e^{i(4j+1)\omega\tau}\right]\lambda_T\left(kD,\beta_j\right)\overbrace{dZ_T(\omega)}^{\text{temperature perturbation}}$$
$$+\frac{a}{2}\sum_{j=-1}^{+1}\left[e^{i(4j-1)\omega\tau}-e^{i(4j+1)\omega\tau}\right]\lambda_p\left(kD,\beta_j\right)\overbrace{\mathbf{RdZ_u}(\omega)\cdot\mathbf{t_j}}^{\text{parallel wind perturbation}}$$
$$-\frac{a}{2}\frac{u}{c}\sum_{j=-1}^{+1}\left[e^{i(4j-1)\omega\tau}+e^{i(4j+1)\omega\tau}\right]\lambda_n\left(kD,\beta_j\right)$$
$$\overbrace{\left[\mathbf{r_1}-\mathbf{t_j}\,\mathbf{r_1}\cdot\mathbf{t_j}\right]}^{\text{normal mean wind}}\cdot\overbrace{\left[\mathbf{RdZ_u}(\omega)-\mathbf{t_j}\,\mathbf{RdZ_u}(\omega)\cdot\mathbf{t_j}\right]}^{\text{normal wind perturbation}}\Bigg\}$$

Here, we define a velocity perturbation vector $\mathbf{dZ_u}=\left[dZ_u,dZ_v,dZ_w\right]$ and the rotated mean flow direction $\mathbf{r_1}=\mathbf{R}\cdot\left[1,0,0\right]$ is the first column of the rotation matrix **R**. The filters $\left(\lambda_T,\lambda_p,\lambda_n\right)$ account for spatial line averaging of temperature and velocity perturbations in parallel and normal to individual measurements paths, see below.

Evaluating velocity responses, we recall that velocity signals from individual measurement paths contribute with the velocity components $\mathbf{s_j}$, and that the combined velocity must be rotated back into the mean flow direction.

$$\mathbf{dZ_{u,s}}(\omega) = \tag{5}$$
$$\mathbf{R^{-1}}\Bigg\{\frac{1}{2a}\sum_{j=-1}^{+1}\left[e^{i(4j-1)\omega\tau}-e^{i(4j+1)\omega\tau}\right]\lambda_T^j\left(kD,\beta_j\right)\mathbf{s_j}dZ_T(\omega)$$
$$+\frac{1}{2}\sum_{j=-1}^{+1}\left[e^{i(4j-1)\omega\tau}+e^{i(4j+1)\omega\tau}\right]\lambda_p^j\left(kD,\beta_j\right)\mathbf{s_j}\overbrace{\mathbf{RdZ_u}(\omega)\cdot\mathbf{t_j}}^{\text{parallel wind perturbation}}$$
$$-\frac{1}{2}\frac{u}{c}\sum_{j=-1}^{+1}\left[e^{i(4j-1)\omega\tau}-e^{i(4j+1)\omega\tau}\right]\lambda_n^j\left(kD,\beta_j\right)$$
$$\mathbf{s_j}\overbrace{\left[\mathbf{r_1}-\mathbf{t_j}\,\mathbf{r_1}\cdot\mathbf{t_j}\right]}^{\text{normal mean wind}}\cdot\overbrace{\left[\mathbf{RdZ_u}(\omega)-\mathbf{t_j}\,\mathbf{RdZ_u}(\omega)\cdot\mathbf{t_j}\right]}^{\text{normal wind perturbation}}\Bigg\}$$

We now introduce an overall perturbation vector $\mathbf{dZ}=\left[dZ_u,dZ_v,dZ_w,dZ_T\right]$ and formally raise the dimension of the rotation matrix to include the temperature signal. It is then possible to organise the response relations as

$$\mathbf{dZ_s}(\omega)=\mathbf{R^{-1}}\left(\mathbf{A}(\omega\tau)-u/c\,\mathbf{B}(\omega\tau)\cdot\mathbf{r_1}\right)\mathbf{RdZ}(\omega) \tag{6}$$

where the matrix **A** and third-order tensor **B** depend on instrument geometry and spatial averaging.

So far we have ignored the on-line correction for temperature distortion by crosswind velocities. The instrument computer corrects each temperature sample by the following formula (Gill 1997)

$$T_{sc}=T_s+\frac{a}{2}\frac{u}{c}\left[\tfrac{3}{4}\left(u_s^2+v_s^2\right)+\tfrac{1}{2}w_s^2\right] \tag{7}$$

which is perfectly correct when firing delays are ignored and equivalent to the correction of Schotanus et al (1983). We linearise the corrected temperature to

$$T_{sc}'=T_s'+a\,u/c\left(\tfrac{3}{4}r_{11}u_s'+\tfrac{3}{4}r_{21}v_s'+\tfrac{1}{2}r_{31}w'\right) \tag{8}$$

Here, we express mean velocity components by the wind speed u and elements of the first column in the rotation matrix $\left(r_{11},r_{21},r_{31}\right)=\mathbf{r_1}$. We can express this crosswind-temperature correction as

$$\mathbf{dZ_{sc}}(\omega)=\mathbf{R^{-1}}\,\mathbf{C}\left(\mathbf{A}(\omega\tau)-u/c\,\mathbf{B}(\omega\tau)\cdot\mathbf{r_1}\right)\mathbf{R}\,\mathbf{dZ}(\omega) \tag{9}$$

with a correction matrix defined by

$$\mathbf{C}=\begin{bmatrix}1&0&0&0\\0&1&0&0\\0&0&1&0\\c_1&c_2&c_3&1\end{bmatrix}\qquad\begin{aligned}c_1&=\tfrac{3}{4}a\,u/c\,r_{11}\\c_2&=\tfrac{3}{4}a\,u/c\,r_{21}\\c_3&=\tfrac{1}{2}a\,u/c\,r_{31}\end{aligned} \tag{10}$$

The spectral matrix is $\chi(\omega)=\left\langle\mathbf{dZ}(\omega)\otimes\mathbf{dZ}^*(\omega)\right\rangle$, where the suffix * denotes complex conjugation and the operator $\otimes$ denotes the outer product. By insertion we see that the instruments spectral response relates to the true spectral matrix by:

$$\chi_{sc}(\omega)=\mathbf{D}\cdot\chi(\omega)\cdot\mathbf{D}^{\dagger} \tag{11}$$

Here, the translation matrix is defined by $\mathbf{D}=\mathbf{R^{-1}}\,\mathbf{C}\left(\mathbf{A}(\omega\tau)-u/c\,\mathbf{B}(\omega\tau)\cdot\mathbf{r_1}\right)\mathbf{R}$ and † denotes its Hermitian conjugate.

The predecessor of the Solent R3 anemometer was the R2 model, which has a similar geometry. The R2 temperature signal was, however, exclusively based on the first measurement path. The main difference in the response analysis is that only the leading term of each sum in the temperature response (4) is included and we drop the over-all factor 1/3. The influence matrices $\mathbf{A_{R2}}$ and $\mathbf{B_{R2}}$ only differ for elements to be multiplied by the last part of the disturbance vector $\mathbf{dZ}=\left[dZ_u,dZ_v,dZ_w,dZ_T\right]$. The R2 temperature distortion by crosswind velocity might have been eliminated by an on-line correction

$$T_{SC,R2}=T_{S,R2}$$
$$+\tfrac{1}{2}a/c\left[\tfrac{7}{8}u^2+\tfrac{5}{8}v^2+\tfrac{1}{2}w^2+\tfrac{\sqrt{3}}{4}uv+\tfrac{1}{2}uw-\tfrac{\sqrt{3}}{2}vw\right] \tag{12}$$

similar to that of the R3 anemometer (7). This feature was, however, not available in the R2 version and the spectral response is evaluated without crosswind-temperature correction.

$$\mathbf{D_{R2}} = \mathbf{R}^{-1}\left(\mathbf{A_{R2}}(\omega\tau) - u/c\,\mathbf{B_{R2}}(\omega\tau)\cdot\mathbf{r_1}\right)\mathbf{R} \tag{13}$$

3.2 *Spatial averaging*

Spatial variations are modelled by the spectral tensor $\Phi(k_1,k_2,k_3)$. Variations are considered as 'frozen turbulence', $f = 2\pi k_1 u$, and the familiar 1-D temporal spectra are found by integration over wave numbers representing lateral and vertical variations. The line-averaging effect is estimated by a 'pseudo-transfer' function, defined as the ratio of spectral response and the ideal spectrum.

$$\mathrm{H}(k_1) = \frac{\iint \Phi(k_1,k_2,k_3)\,\mathrm{sinc}^2(\mathbf{k}\cdot\mathbf{t}\,D/2)\,dk_2dk_3}{\iint \Phi(k_1,k_2,k_3)\,dk_2dk_3} \tag{14}$$

The weight function is defined by $\mathrm{sinc}^2(x) \equiv \sin^2(x)/x^2$ where the argument is the scalar product of the wave-number vector $\mathbf{k} = (k_1,k_2,k_3)$ and path-direction unit vector **t** multiplied by half the measurement-path length $D/2$. Fortunately, the measurement paths of the R3 anemometer cross each other at the centre, so we do not have to consider path displacement, as in the treatment of the Kaijo Denki A-type sonic by Kaimal et al. (1968).

The pseudo-transfer function depends on the signal component and measurement-path direction. The spectral tensor is not accurately known, but it is argued that line averaging over short measurement paths is only significant well into the inertial sub-range, where simple isotropic models suffice. Such models are

$$\begin{aligned}\Phi_{\mathrm{U_iU_j}}(k_1,k_2,k_3) &\propto k^{-17/3}\left(\delta_{i,j}k^2 - k_i k_j\right)\\ \Phi_{\mathrm{TT}}(k_1,k_2,k_3) &\propto k^{-11/6}\end{aligned} \tag{15}$$

where $k^2 = k_1^2 + k_2^2 + k_3^2$ and $\delta_{i,j}$ is Kronecker's delta. In general, the measurement path will have an oblique angle relative to the wind direction, $\beta = \cos^{-1}\left|\mathbf{t_j}\cdot\mathbf{r_1}\right|$. The temperature transfer functions for this condition is

$$\begin{aligned}\mathrm{H_T}(k_1,\beta) &= \frac{2\Gamma\left(\frac{1}{3}\right)k_1^{5/3}}{3\pi^{1/2}\Gamma\left(\frac{5}{6}\right)}\\ &\cdot\int_0^\infty \left(k_1^2+k_3^2\right)^{-4/3}\mathrm{sinc}^2\left[\tfrac{1}{2}\left(k_1\cos\beta + k_3\sin\beta\right)D\right]dk_3\end{aligned} \tag{16}$$

where integration over vertical wave numbers have to be numerical. Similarly, for velocity perturbations parallel to the measurement paths

$$\begin{aligned}\mathrm{H}_{u,p}(k_1,\beta) = &\\ &\frac{16\Gamma^2\left(\frac{1}{3}\right)\Gamma\left(\frac{1}{6}\right)k_1^{5/3}}{3\left(\begin{array}{l}5\pi 2^{1/3}\Gamma\left(\frac{2}{3}\right)\Gamma\left(\frac{1}{6}\right)(7-4\cos 2\beta)\\ -16\Gamma^2\left(\frac{1}{3}\right)\Gamma\left(\frac{1}{6}\right)\sin 2\beta + 6\pi^{3/2}\Gamma\left(\frac{1}{3}\right)(7+4\cos 2\beta)\end{array}\right)}\\ &\cdot\int_0^\infty\left[(7-4\cos 2\beta)k_1^2 - (8\sin 2\beta)k_1k_3 + (7+4\cos 2\beta)k_3^2\right]\\ &\left(k_1^2+k_3^2\right)^{-7/3}\mathrm{sinc}^2\left[\tfrac{1}{2}\left(k_1\cos\beta + k_3\sin\beta\right)D\right]dk_3\end{aligned} \tag{17}$$

and crosswind to the measurement path

$$\begin{aligned}\mathrm{H}_{u,n}(k_1,\beta) = &\\ &\frac{16\Gamma^2\left(\frac{1}{3}\right)\Gamma\left(\frac{1}{6}\right)k_1^{5/3}}{3\left(\begin{array}{l}15\pi 2^{1/3}\Gamma\left(\frac{2}{3}\right)\Gamma\left(\frac{1}{6}\right) + 40\pi^{1/2}\Gamma\left(\frac{1}{3}\right)\Gamma\left(\frac{1}{6}\right)\Gamma\left(\frac{5}{6}\right)\cos^2\beta\\ +16\Gamma^2\left(\frac{1}{3}\right)\Gamma\left(\frac{1}{6}\right)\sin 2\beta + 6\pi^{3/2}\Gamma\left(\frac{1}{3}\right)(7-4\cos 2\beta)\end{array}\right)}\\ &\cdot\int_0^\infty\left[(7+4\cos 2\beta)k_1^2 + (8\sin 2\beta)k_1k_3 + (7-4\cos 2\beta)k_3^2\right]\\ &\left(k_1^2+k_3^2\right)^{-7/3}\mathrm{sinc}^2\left[\tfrac{1}{2}\left(k_1\cos\beta + k_3\sin\beta\right)D\right]dk_3\end{aligned} \tag{18}$$

Figure 1 shows three types of pseudo-transfer functions for the minimum, mean and maximum angles between measurement paths and wind vectors in the horizontal plane together with the simple $\mathrm{sinc}^2\left(\frac{1}{2}kD\right)$ filter. The functions are not very different from the simple case, except when the measurement path is nearly perpendicular to the wind.

Turbulent fluxes do not exist in isotropic turbulence. As an approximation Larsen et al. (1993) estimated the pseudo-transfer function for mixed relations by the product of transfer functions estimated by isotropic fields. We extend this approximation to transfer function for cross-spectra signals measured by different paths:

$$\mathrm{H_{XY}}(k,\beta_1,\beta_2) \approx \sqrt{\mathrm{H_X}(k,\beta_1)}\sqrt{\mathrm{H_Y}(k,\beta_2)} \tag{19}$$

This assumption allows us to estimate the correction factors used in the response equations **(4)** and **(5)**

$$\begin{aligned}\lambda_T^j(kD,\beta_j) &= \sqrt{\mathrm{H_T}\left(\omega/u\,D,\cos^{-1}\left|\mathbf{t_j}\cdot\mathbf{r_1}\right|\right)}\\ \lambda_p^j(kD,\beta_j) &= \sqrt{\mathrm{H_{u,p}}\left(\omega/u\,D,\cos^{-1}\left|\mathbf{t_j}\cdot\mathbf{r_1}\right|\right)}\\ \lambda_n^j(kD,\beta_j) &= \sqrt{\mathrm{H_{u,n}}\left(\omega/u\,D,\cos^{-1}\left|\mathbf{t_j}\cdot\mathbf{r_1}\right|\right)}\end{aligned} \tag{20}$$

3.3 *Digital sampling*

Each measurement cycle of the Solent R3 anemometer takes $\Delta\tau$=10 ms equal to a sample frequency of 100 Hz and the instrument output is the block average of an optional number of samples N ranging from 1 to 250. We model the combined effect of this digital sampling as

$$\bar{S}_x(\omega) = \left[\frac{\sin N\omega\Delta\tau/2}{N\sin\omega\Delta\tau/2}\right]^2 \sum_{m=-\infty}^{+\infty} S_x\left(\omega + m\,2\pi/\Delta\tau\right) \qquad (21)$$

where the sum includes alias contributions and the factor in front is the effect of averaging a sequence of N samples. We assume that $N = 5$ equal to an output rate of 20 Hz is a popular choice.

4. EXAMPLE

Following Larsen et al. (1993) we model the spectral matrix $\chi(\omega)$ by conventional surface-layer scaling (Kaimal, 1972) and examine the instrument response by Eqn. (11). The temperature signal is the most sensitive one, in particular for near-neutral conditions, where the true spectrum may be arbitrarily small compared to the velocity disturbances. This worst-case situation is shown in Figure 2. The directional dependence illustrated by the shaded areas is both related to variable line-averaging effect and to the shift of the wind vector relative to the pulse-firing pattern. The pulse-delay effect adds a significant high-frequency component to the temperature signal, which is moderated by the line averaging effect, as expected. Furthermore, the figure shows how aliasing contaminates the 1-10 Hz range by the false high-frequency response. This end result is also shown for the earlier R2 model. The R2 anemometer has no temperature correction and its temperature response is biased at all frequencies. The spectrum sampled by the R2 model follows the ideal slope to higher frequencies. Not knowing the true spectrum, the casual user might not realize that the R3 measurements are more accurate. Figure 3 shows that the heat-flux responses for the same test case are much better measured by the R3 anemometer.

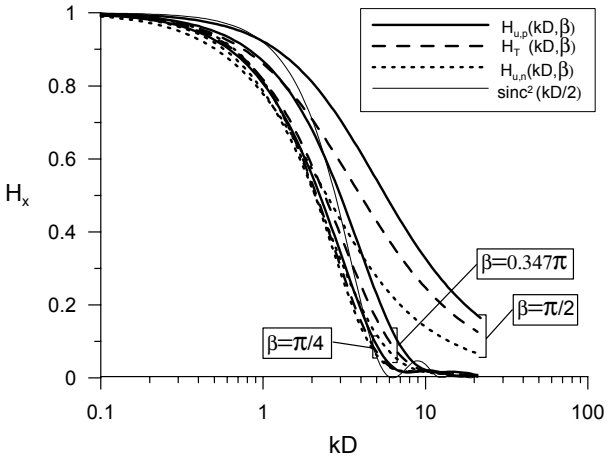

Figure 1 Pseudo-transfer functions for along-path velocity (solid line), temperature (dashed line), and cross-path velocity (dotted line) shown for various angles between wind and measurement path, β.

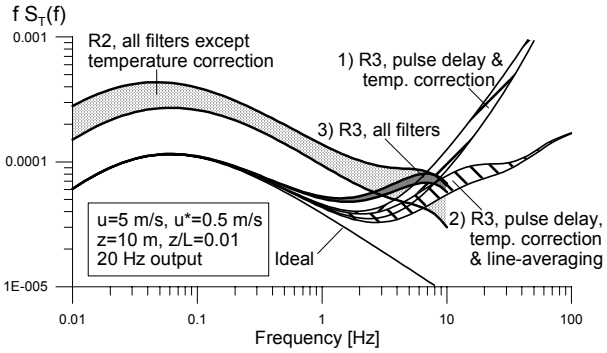

Figure 2 Temperature power spectrum for weak wind and near-neutral conditions.

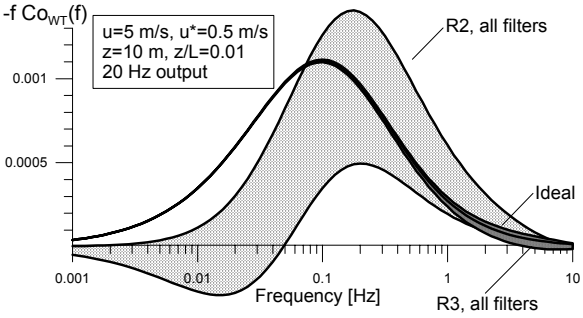

Figure 3 Heat flux spectrum for weak wind and near-neutral conditions.

Acknowledgement

This work is part of the AUTOFLUX project funded by the European Commission under contract no. MAS3-CT97-0108.

References

Gill, 1997: Omnidirectional (R3) & asymmetric (R3A) research ultrasonic anemometer, *User manual and product specification*, Doc. No. 1210-PS-0002 Issue. 3, Gill Instruments Ltd. UK

Kaimal, J.C., J.C. Wyngaard, Y. Izumi, O.R. Coté, 1972: Spectral characteristics of surface layer turbulence. *Quart. J. R. Soc.*, **98**, 563 - 589.

Kaimal, J.C., and J. E. Gaynor, 1991: Another look at sonic thermometry, *Boundary-Layer Meteorol.* **56**, 401-410.

Larsen, S.E., J.B. Edson, C.W. Fairall and P.G. Mestayer, 1993: Measurement of temperature spectra by a sonic anemometer. *J. Atmos. Ocean. Technol.*, **10**, 345-354.

Schotanus, P., F.T.M. Niuwstadt, and H.A.R. de Bruin, 1983: Temperature measurement with a sonic anemometer and application to heat and moisture fluxes, *Boundary-Layer Meteorol.* **26**, 81-93.